Scientia Iranica B (2023) 30(5), 1612–1624

Sharif University of Technology
Scientia Iranica
Transactions B: Mechanical Engineering
http://scientiairanica.sharif.edu

Research Note

Reverse flow analysis of hybrid nanofluid MHD mixed convection flow in a vertical cylindrical annulus: An exact solution

A. Shakiba[a,b], and A. Baradaran Rahimi[a,*]

a. *Department of Mechanical Engineering, Ferdowsi University of Mashhad, P.O. Box 91775-1111, Mashhad, Iran.*
b. *Faculty of Engineering, Ferdowsi University of Mashhad, P.O. Box 91775-1111, Mashhad, Iran.*

Received 23 January 2022; received in revised form 7 May 2022; accepted 18 January 2023

KEYWORDS
Reverse flow;
Vertical cylindrical annulus;
Hybrid nanofluid;
Moving walls;
Magnetohydrodynamics (MHD);
Mixed convection heat transfer;
Suction/injection;
Exact solution.

Abstract. In recent decades, reverse flow analysis in mixed convection flow has attracted the attention of many researchers owing to its applications in the design of medical and engineering systems. The presence of reverse flow is unfavorable in many respects; therefore, it is crucial to find values of critical parameters affecting reverse flow to eliminate it. In this paper, the thermal and hydrodynamic behaviors of Multi Walled Carbon Nanotube (MWCNT)-Fe_3O_4 hybrid nanofluid are explored in a vertical cylindrical annulus and in the adjacency of radial magnetic field by achieving the results of exact solution. Furthermore, effective factors in reverse flow are investigated, considering the effects of wall movement and suction/injection on it. The range of changes in the values of governing parameters includes constant velocity of cylinder walls $A = 0 - 10$, $B = 0 - 10$, mixed convection parameter $\eta = -1500 - 1500$, dimensionless temperature difference ratio $\xi = 0 - 1$, Hartman number $Ha = 0 - 50$, suction/injection $S = -6 - 6$, concentration of nanocomposite particles at $\varphi = 0 - 0.3\%$, and radius ratio $\lambda = 2 - 10$. Results reveal that hybrid nanofluid enhances heat transfer rate. Moreover, by changing the above-mentioned parameters and selecting appropriate values for them, the flow, heat transfer, and occurrence of reverse flow can be optimally controlled. Meanwhile, such parameters as Ha, S, and ξ perform better in eliminating reverse flow.

1. Introduction

Improving the efficiency and performance of thermal devices ensures saving energy, diminishes the size of devices, and accordingly reduces the cost of materials and their construction. Many researchers have seriously studied mixed convection heat transfer in concentric cylinders on account of its applications in manufacturing industries, heat exchangers, cooling systems of electronic appliances, solar collectors, food processes, nuclear reactors, extrusion process, polymer coating inside the pipe, the simulation of a train passing through a long tunnel, excavating operations, and other similar cases [1–3]. It should be stated that easy design and production of annulus and its low-pressure drop can be regarded as some of its advantages. Needless to apply energy or work from outside of the system, a significant amount of heat can be transferred from a small cross-section in these thermal devices. Oni et al. [4] analyzed the potentials of dual streaming in electroosmotic fluid flow and heat transfer in a vertical micro annulus considering the effect of Joule heating.

*. *Corresponding author.*
E-mail address: rahimiab@yahoo.com (A. Baradaran Rahimi)

doi: 10.24200/sci.2023.59823.6446

After solving governing equations, findings revealed that skin-friction and heat transfer for normal streaming potential enhanced the function of magnitude of electroosmotic parameter and Joule heating factor. Jha and Gambo [5] studied the effect of an oscillating time-dependent pressure gradient on Dean flow in an annulus theoretically. The results of utilized Laplace transform technique indicated that applying suction on perforated walls and increasing oscillation frequency would reduce the effectiveness of skin frictions on both walls of cylinder. Additionally, further research [6–9] managed to investigate fluid flow and heat transfer in an annulus. Amouzadeh et al. [10] analytically surveyed the impact of suction/injection on MHD fluid flow in a vertical annulus by considering radial heat generation or absorption with the aim of cooling electronic equipment. They showed that suction and heat absorption parameters increased Nusselt number, while injection and heat generation parameters reduced it.

One of the new types of nanofluids is hybrid nanofluid. It refers to any nanofluid whose structure incorporates more than one type of nanoparticle [11–14]. By studying nanofluid mixed convection heat transfer within a vertical annulus, Malvandi et al. [15] discovered that enhancing mixed convection parameter increased velocity and temperature near the hot wall. Moreover, buoyancy force had a negative effect on system efficiency.

Shakiba and Baradaran Rahimi [16] examined the behavior of mixed convection heat transfer of the fluid, which had electrical conductivity, in a vertical cylindrical annulus by taking into account the effects of wall movement and radial magnetic field. Through obtaining the results of exact solution, they realized that Nusselt number and shear stress decreased on inner cylinder wall following increase in Hartman number. Moreover, increasing λ enhances Nusselt number and reduces shear stress on the inner cylinder wall. In another study, considering the effects of suction/injection and the use of CuO-Water nanofluid in a vertical annulus, Shakiba and Bradaran Rahimi [17] came to this conclusion that enhancing nanoparticles volume fraction caused heat transfer rate to heighten and platelet-shaped nanoparticles had the highest heat transfer rate. Besides, they found that in different situations of wall movement, the enhancement of mixed convection parameter increased heat transfer rate and shear stress on the inner cylinder wall.

In recent decades, the analysis of reverse flows in mixed convection flow has attracted the attention of many scholars because of its applications to medicine and engineering [18–20]. Reverse flow in an annulus may occur on the side of cylinders' walls or in the distance between them. With the analytical study of mixed convection flow in a vertical annulus, Barletta [21] realized that reverse flow occurred at certain values of mixed convection parameters. Moreover, he found that the value of this parameter depended on radius ratio. In a theoretical study, by obtaining the results of exact solution for a vertical channel, Jha and Oni [22] concluded that the formation of reverse flow increased on the walls following the inclusion of nonlinear density variation with temperature. Furthermore, results indicated that the formation of reverse flow near the wall could be optimized through appropriate control parameters. In another study, Jha and Aina [23] reported that the formation of reverse flow was less likely to happen in the cold wall of microchannel by increasing Knudsen number. By attaining the results of exact solution for mixed convection flow within a vertical channel, Jha and Oni [24] threw light on the fact that reverse flow increased by enhancing viscosity variation parameter around the cold region. Besides, the wall temperature ratio played a crucial role in reducing reverse flow.

Apart from the above-mentioned research, a limited number of articles have discussed the effective factors in the reverse flow in a vertical annulus. The novelty of this research is to establish analytical solutions to study the effective factors in reverse flow in adjacency of the radial magnetic field by considering the mixed convection heat transfer regime of hybrid nanofluid in a vertical annulus geometry. This study intends to comparatively elucidate the importance of eliminating reverse flow in annulus geometry through investigating various parameters, including thermal boundary conditions, internal and external cylinders' walls velocity, suction/injection, magnetic field, volume fraction of hybrid nanoparticles, and radius ratio.

2. Problem statement

The annulus geometry consisting of two vertical and concentric cylinders in a cylindrical coordinate system along with the way of applying boundary conditions is illustrated in Figure 1. The radii of inner and outer cylinders are equal to a and b, respectively, and the temperature of inner and outer cylinders equals to T_1 and T_2, respectively. Walls of the inner and outer cylinders move at constant velocities of Au_0 and Bu_0, respectively, in which u_0 is reference velocity and A and B are constant numbers so that their change causes the velocity of inner and outer cylinder walls to alter as well. The fluid is suctioned/injected on inner and outer cylinder walls and it is affected by a radial magnetic field with the magnitude of $B_0 a/r$ in the space between two cylinders.

3. Governing equations and boundary conditions

Regardless of viscosity dissipation and axial conduction

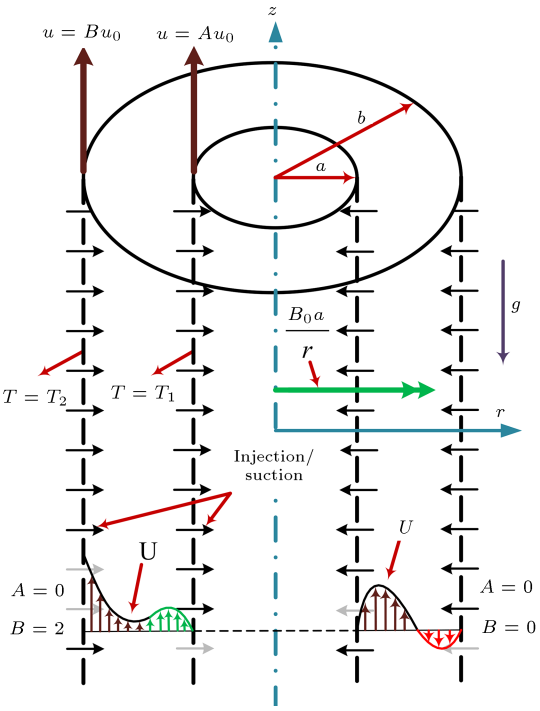

Figure 1. Problem geometry, coordinate system, and the applied boundary conditions.

of the fluid and the wall, the equations of continuity, momentum, and energy are solved according to Relations (1)–(3) [17]. In these equations, No Slip condition and Boussinesq approximation are used on the cylinder walls and the flow is regarded as steady, laminar, Newtonian, incompressible and fully developed. Considering the infinite length for annulus, all physical parameters of the problem are a function of r, except the pressure which is a function of z.

Continuity equation:

$$\frac{1}{r}\frac{d}{dr}(rV) = 0. \tag{1}$$

Momentum equation:

$$V\frac{du}{dr} = -\frac{1}{\rho_{hnf}}\frac{dp}{dz} + \frac{\mu_{hnf}}{\rho_{hnf}}\frac{1}{r}\frac{d}{dr}\left(r\frac{du}{dr}\right) + g\beta_{hnf}(\Delta T) - \frac{\sigma_{hnf}B_m^2 u}{\rho_{hnf}}. \tag{2}$$

Energy equation:

$$\frac{k_{hnf}}{(\rho C_p)_{hnf}}\frac{1}{r}\frac{d}{dr}\left(r\frac{dT}{dr}\right) = V\frac{dT}{dr}. \tag{3}$$

In Eqs. (1)–(3), ρ_{hnf}, $(C_p)_{hnf}$, σ_{hnf}, and β_{hnf} are density, heat capacity, electrical conductivity, and thermal expansion coefficient of hybrid nanofluid, respectively. The boundary conditions of this problem are also as follows:

$$r = a, \quad u = Au_0, \quad T = T_1,$$
$$r = b, \quad u = Bu_0, \quad T = T_2. \tag{4}$$

By integrating Relation (1) and using boundary condition $(r = a, V_r = -V_0)$, velocity component in the radial direction is attained in terms of $V_r = \frac{-aV_0}{r}$. Furthermore, axial velocity component (V_z) is denoted by (u).

Dimensionless parameters defined in the present work are in the form of Relation (5):

$$R = \frac{r}{a}, \quad \lambda = \frac{b}{a}, \quad Z = \frac{z}{ReD_h},$$
$$U = \frac{u}{u_0}, \quad \theta = \frac{T - T_0}{T_1 - T_0}, \quad P = \frac{p}{\rho_{hnf}u_0^2},$$
$$Gr = \frac{g\beta_f \Delta T D_h^3}{\nu_f^2}, \quad Pr = \frac{\nu_f}{\alpha_{T,f}}, \quad Ha = B_0 D_h\sqrt{\frac{\sigma_f}{\mu_f}},$$
$$\xi = \frac{T_2 - T_0}{T_1 - T}, \quad Re = \frac{u_0 D_h}{\nu_f}, \quad \eta = \frac{Gr}{Re}. \tag{5}$$

In the above relations, T_0 is regarded as reference temperature. Besides, parameters D_h, ν_f, α_T, B, and ΔT are hydraulic diameter, kinematic viscosity, thermal diffusivity coefficient, magnetic field, and temperature difference, respectively. They are defined according to the following:

$$D_h = 2(b - a), \quad \nu_f = \frac{\mu_f}{\rho_f}, \quad \alpha_{T,f} = \frac{k_f}{\rho_f C_{p,f}},$$
$$B_m = \frac{B_0 a}{r}, \quad \Delta T = T_1 - T_0. \tag{6}$$

Using dimensionless parameters defined in Relation (5), the equations governing the problem become dimensionless in the form of Relations (7) and (8).

Momentum equation:

$$-\frac{S}{R}\frac{d}{dR}U(R) - \frac{\mu_{hnf}}{\mu_f}\frac{\rho_f}{\rho_{nf}}\frac{1}{R}\frac{d}{dR}\left(R\frac{d}{dR}U(R)\right) + \frac{1}{4(\lambda - 1)^2}\left[\frac{dP}{dZ} + \frac{Ha^2}{R^2}\frac{\sigma_{hnf}}{\sigma_f}\frac{\rho_f}{\rho_{hnf}}U(R) - \frac{\beta_{hnf}}{\beta_f}\eta\theta(R)\right] = 0. \tag{7}$$

Energy equation:

$$\frac{k_{hnf}}{k_f}\frac{(\rho C_p)_f}{(\rho C_p)_{hnf}}\frac{1}{Pr}\frac{d}{dR}\left(R\frac{d}{dR}\theta(R)\right) + S\frac{d}{dR}\theta(R) = 0. \tag{8}$$

In these equations, μ_{hnf} and k_{hnf} are kinematic viscosity and thermal conductivity of hybrid nanofluid,

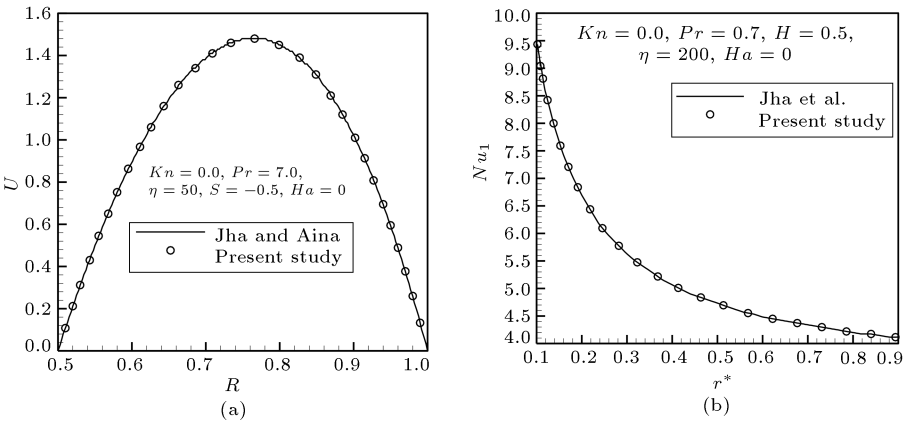

Figure 2. Validation (a) comparison of the fully developed dimensionless velocity profile with Ref. [25] and (b) comparison of the present study's Nusselt number on inner cylinder of annulus with Ref. [26].

respectively. Dimensionless boundary conditions are given in the following:

$$R = 1, \quad U = A, \quad \theta = 1,$$

$$R = \lambda, \quad U = B, \quad \theta = \xi. \tag{9}$$

By employing Relations (10) and (11), at any cross-section of annulus, the mean velocity (u_0) is considered reference velocity and the constant non-dimensional volumetric flow rate (Q) can be calculated. In addition, the balk temperature can be computed through Eq. (12).

$$u_0 = u_m = \frac{\int_a^b urdr}{\int_a^b rdr}, \tag{10}$$

$$Q = \int_1^\lambda RU(R)\,dR = \int_1^\lambda RdR = \frac{1}{2}\left(\lambda^2 - 1\right), \tag{11}$$

$$\theta_b = \frac{T_b - T_0}{T_1 - T_0} = \frac{\int_1^\lambda RU(R)\,\theta(R)\,dR}{\int_1^\lambda RU(R)\,dR}. \tag{12}$$

By utilizing the boundary conditions presented in Relation (9) and solving Eqs. (7)–(8), the results of exact solution for velocity and temperature are represented as:

$$\theta(R) = \delta_2 + \delta_3 R^{\delta_1}$$

$$U(R) = C_1 R^{\frac{\delta_4+\delta_5}{\delta_6}} + C_2 R^{\frac{\delta_4-\delta_5}{\delta_6}} + \delta_{11}(\delta_9 R^{\delta_1} + \delta_{10})R^2. \tag{13}$$

Moreover, Nusselt number and dimensionless shear stress are in the form of Relations (14) and (15) are shown in Box I. In the above relations, C_1, C_2 and $\delta_1 - \delta_{11}$ are the constant coefficients that are defined according to Relation (16) as shown in Box II.

4. Credibility

In order to validate the viability of the used method, Figure 2(a) shows the dimensionless velocity profile for the fully developed flow in a vertical annulus and in the absence of magnetic field compared with the results of exact solution in the study of Jha and Aina [25]. In this comparison, the cylinders are in the stationary state and Knudsen number is considered $Kn = 0$. Additionally, the comparison of Nusselt number values obtained for the inner cylinder wall with the results of Jha et al. [26] is presented in Figure 2(b). These comparison results are presented for Nusselt number at different radius ratios and by considering the suction/injection on the walls. It can be demonstrated that the matching of the results in both figures is acceptable.

5. Hybrid nanofluid thermo-physical properties

Hybrid nanofluid, which consists of a combination of two or more different nanoparticles, is one of the new types of nanofluids that has received recognition in recent years for increasing the rate of heat transfer [27]. The present study aims to use the hybrid nanofluid of Multi-Wall Carbon Nanotube (MWCNT)-Fe_3O_4 in base fluid. It should be noted that since the size of nanoparticles is very small, slipping velocity between them and continuous phase are disregarded. It is also assumed that nanoparticles and base fluid are in a thermal equilibrium state. The conducted surveys indicate that in general, much less research has been done on measuring the properties of hybrid nanofluids and there is no clear relation for calculating the thermophysical properties of these new suspensions. Therefore, according to Table 1, laboratory data [28,29] related to the hybrid nanofluid properties of MWCNT-Fe_3O_4 have been utilized in this study.

$$Nu|_{R=1}=\frac{-2\left(\lambda-1\right)}{\theta|_{R=1}-\theta_b}\frac{k_{hnf}}{k_f} \qquad \left.\frac{d\theta}{dR}\right|_{R=1}=\frac{2k_{hnf}\delta_3\delta_1(\lambda-1)}{k_f(-1+\theta_b)},$$

$$Nu|_{R=\lambda}=\frac{2\left(\lambda-1\right)}{\theta|_{R=\lambda}-\theta_b}\frac{k_{hnf}}{k_f} \qquad \left.\frac{d\theta}{dR}\right|_{R=\lambda}=\frac{2\left(\lambda-1\right)k_{hnf}\delta_3\lambda^{\delta_1}\delta_1}{k_f\lambda\left(\xi-\theta_b\right)}, \tag{14}$$

$$\tau|_{wall}=\frac{\mu_{hnf}}{\mu_f}\left.\frac{dU}{dR}\right|_{wall}=\begin{cases}\tau_1=\frac{\delta_{10}(\delta_{11}(\delta_1+2)+2\delta_9)\delta_6+\delta_4(C_1+C_2)+\delta_5(C_1-C_2)}{\delta_6}\\ \tau_\lambda=\frac{C_2\lambda^{\frac{\delta_4-\delta_5-\delta_6}{\delta_6}}(\delta_4-\delta_5)+C_1\lambda^{\frac{\delta_4+\delta_5-\delta_6}{\delta_6}}(\delta_4+\delta_5)+\delta_6\delta_{10}\left(\delta_{11}(\delta_1+2)\lambda^{\delta_1+1}+2\lambda\delta_9\right)}{\delta_6}\end{cases} \tag{15}$$

Box I

$$C_1=\frac{\left(\left(-\delta_7-\delta_8\right)\delta_9+A\right)\lambda^{\frac{\delta_4-\delta_5}{\delta_6}}+\lambda^{\delta_1}\lambda^2\delta_7\delta_9+\lambda^2\delta_8\delta_9-B}{-\lambda^{\frac{\delta_4+\delta_5}{\delta_6}}+\lambda^{\frac{\delta_4-\delta_5}{\delta_6}}},$$

$$C_2=\frac{\left(\left(\delta_7+\delta_8\right)\delta_9-A\right)\lambda^{\frac{\delta_4+\delta_5}{\delta_6}}-\lambda^{\delta_1}\lambda^2\delta_7\delta_9-\lambda^2\delta_8\delta_9+B}{-\lambda^{\frac{\delta_4+\delta_5}{\delta_6}}+\lambda^{\frac{\delta_4-\delta_5}{\delta_6}}},$$

$$\delta_1=-\frac{PrS\alpha_f}{\alpha_{hnf}}, \qquad \delta_2=\frac{\lambda^{\delta_1}-\xi}{\lambda^{\delta_1}-1}, \qquad \delta_3=\frac{\xi-1}{\lambda^{\delta_1}-1}, \qquad \delta_4=S\mu_f\rho_{hnf}\sigma_f\left(1-\lambda\right),$$

$$\delta_5=\sqrt{\left(S^2\mu_f\rho_{hnf}^2\sigma_f^2(\lambda-1)^2+Ha^2\mu_{hnf}\rho_f^2\sigma_f\right)\mu_f\sigma_f},$$

$$\delta_6=2\mu_{hnf}\rho_f\sigma_f\left(\lambda-1\right),$$

$$\delta_7=\left(\lambda-1\right)^2\left(S\mu_f\rho_{hnf}+2\mu_{hnf}\rho_f\right)\sigma_f-\frac{Ha^2\sigma_{hnf}\rho_f\mu_f}{8},$$

$$\delta_8=\left(\lambda-1\right)^2\left(\delta_1+2\right)\left(\mu_{hnf}\rho_f\left(\delta_1+2\right)+S\mu_f\rho_{hnf}\right)\sigma_f-\frac{Ha^2\sigma_{hnf}\rho_f\mu_f}{4}$$

$$\delta_9=-2\delta_7\delta_3\beta_{hnf}\eta, \qquad \delta_{10}=\left(-\eta\beta_{hnf}\delta_2+P\beta_f\right)\delta_8, \qquad \delta_{11}=\frac{\sigma_f\mu_f\rho_{hnf}}{8\delta_8\beta_f\delta_7}. \tag{16}$$

Box II

Table 2 represents the thermophysical properties of Fe_3O_4 and MWCNT separately [28,29].

Other thermophysical properties of hybrid nanofluid can be obtained using the following relations [29]:

$$\alpha_{hnf}=\frac{k_{hnf}}{\left(\rho C_p\right)_{hnf}},\rho_{hnf},$$

$$\beta_{hnf}=\left(1-\phi\right)\left(\rho\beta\right)_{bf}+\phi(\rho\beta)_{np},$$

$$\beta_{np}=\frac{\left(\beta\phi\right)_{MWCNT}+\left(\beta\phi\right)_{Fe_3O_4}}{\phi_{MWCNT}+\phi_{Fe_3O_4}}$$

$$\sigma_{hnf}=\sigma_{bf}\left(1+\frac{3\left(\frac{\sigma_{np}}{\sigma_{bf}}-1\right)\phi}{\left(\frac{\sigma_{np}}{\sigma_{bf}}+2\right)-\left(\frac{\sigma_{np}}{\sigma_{bf}}-1\right)\phi}\right). \tag{17}$$

Since the order of σ_{MWCNT} (O (10^{-7})) is not comparable with $\sigma_{Fe_3O_4}$ (O (10^4)), σ_{np} is considered equal to the electrical conductivity of Fe_3O_4 nanoparticles.

6. Results and discussion

This study aims to identify effective factors in produc-

Table 1. Thermophysical properties of hybrid nanofluid of MWCNT-Fe_3O_4 in different volume fractions [28,29].

φ (%)	$\rho\left(\frac{kg}{m^3}\right)$	$k\left(\frac{W}{m.K}\right)$	$\mu\left(\frac{kg}{m.s}\right)$	$C_p\left(\frac{J}{kg.K}\right)$
Base fluid ($\varphi = 0.0$)	998.5	0.602	0.79	4182
0.1	1002.34	0.6734	0.91	4182.66
0.3	1010.04	0.6856	1.01	4183.99

Table 2. Thermophysical properties of Fe_3O_4 and MWCNT [28,29].

Nano particle	ρ (kg/m^3)	k (W/m.K)	C_p (J/(kg.K))	β (1/K)
MWCNT	2100	3000	711	4.2×10^{-5}
Fe_3O_4	5810	6	670	1.3×10^{-5}

ing and overcoming reverse flow for annulus geometry.

6.1. Effective factors on producing reverse flow

Changing the velocity of walls can be regarded as one of the effective factors in reverse flow. Therefore, obtaining critical velocity values for moving walls is of great importance. Critical A and B values, which represent the critical velocities of inner and outer cylinder walls, are given in Table 3. This table indicates that increasing wall velocity to more than critical values will cause reverse flow. The values of Nusselt number and shear stress on the walls of inner and outer cylinders in critical situations are also presented in this table. Critical radius (R_{cr}), whose values are given in Table 3, depicts the radius at which reverse flow occurs.

The effects of changes in η on U profile in radial distance between the two inner and outer cylinders are depicted in Figure 3. Inner and outer cylinder walls are taken as hot and cold walls, respectively, when $\eta > 0$. In such conditions, buoyancy force as a dominant force increases velocity near the hot wall; further, increase in the buoyancy force reduces velocity near the cold wall and reverse flow happens eventually. The situation $\eta < 0$ is also related to the condition in which hot and cold walls are replaced. In this situation, outer and inner cylinder walls are regarded as hot and cold walls, respectively. Clearly, the analyses of previous states are also valid for this situation and as η decreases, reverse flow increases. Moreover, according to Figure 3, there is a point that is obtained from the intersection of lines. This point, which is located near the center of radial distance between two cylinders ($R \cong 1.55$), indicates the independence of dimensionless velocity

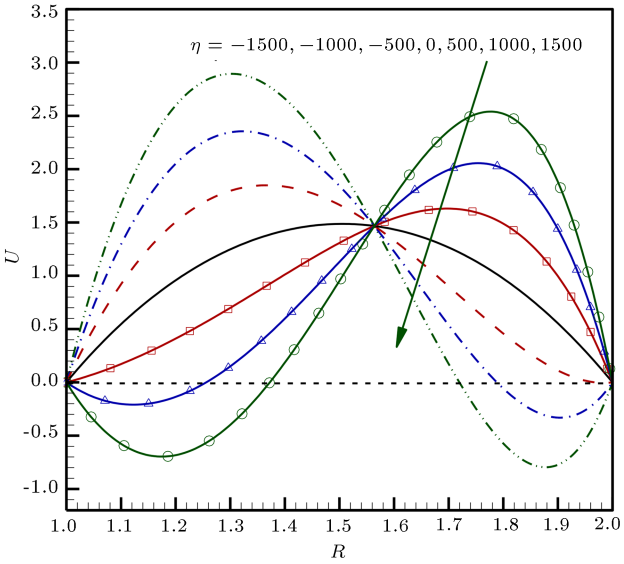

Figure 3. Dimensionless velocity at different values of η parameter in $\xi = 0.2$, $A = 0.0$, $B = 0.0$, $Ha = 5.0$, $S = -1.0$, and $\lambda = 2.0$.

profile from η. This point shows the place where the local temperature of hybrid nanofluid equals reference temperature. In other words, dimensionless temperature is zero at this point. As a matter of fact, this point displays the boundary between points with lower temperature than reference temperature and points with higher temperature than that.

Concerning Figure 3, finding critical values related to η, in which reverse flow occurs, is of great importance. Similar to Figure 3, critical points for mixed convection parameter are presented in Table 4. The values of Nusselt number and shear stress on inner

Table 3. Critical values for wall velocity along with Nusselt number and dimensionless shear stress $\xi = 0.2$, $Ha = 5.0$, $S = -1.0$, $\lambda = 2.0$.

	A_{cr}	B_{cr}	R_{cr}	Nu_1	τ_1	Nu_λ	τ_λ
$\eta = 100$	3.191	0.000	2.000	2.964	−8.089	6.625	0.000
	0.000	3.093	1.000	0.626	0.000	15.360	11.628
	3.120	3.120	1.513	0.821	−16.964	10.983	17.860

Table 4. Critical values for the parameter η along with Nusselt number and dimensionless shear stress in $\xi = 0.2$, $Ha = 5.0$, $S = -1.0$, and $\lambda = 2.0$.

	η_{cr}	Re_cr	Nu_1	τ_1	Nu_λ	τ_λ
$A = 0$, $B = 0$	−638.263	1.000	0.926	0.000	9.959	−19.124
	455.366	2.000	1.758	13.596	7.397	0.000

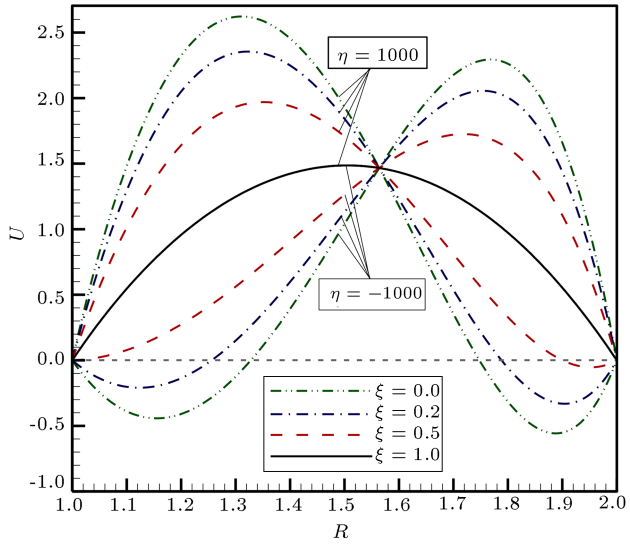

Figure 4. Dimensionless velocity at different values of ξ in $\eta = \mp 1000$, $A = 0.0$, $B = 0.0$, $Ha = 5.0$, $S = -1.0$, $\lambda = 2.0$.

and outer cylinder walls have also been demonstrated. The results of this table shed light on the fact that in the case of positive η, reverse flow happens if it is larger than η_{cr}. In the negative case for η, this event takes place when η is smaller than η_{cr}. Regarding the above results, factors such as wall velocity (A,B) and the mixed convection parameter (η) are among the factors creating reverse flow in annulus geometry.

6.2. The variation of effective factors in eliminating reverse flow

6.2.1. Thermal boundary conditions

Dimensionless velocity changes in the radial distance of annulus at different values of parameter ξ in two states of $\eta = \mp 1000$ are shown in Figure 4. The temperatures of inner and outer cylinder walls and reference temperature are assumed T_1, T_2, and T_0, respectively. Furthermore, it is supposed that $T_1 \geq T_2$. When $\xi = 0$, the asymmetric channel wall heating occurs and the inner and outer cylinder walls have the highest temperature difference. Inner and outer cylinder walls approach the condition of symmetrical temperature as ξ parameter increases and gets close to 1. Reverse flow happens near the outer cylinder wall when $\xi = 0$ and $\eta = +1000$. As can be observed, reverse flow decreases with the enhancement of ξ parameter and it disappears as ξ parameter approaches 1 (symmetric channel wall heating). As a matter of fact, when η is constant, the difference in the temperature of two walls lessens and velocity profile turns to the symmetrical situation with increase in the value of ξ parameter. Besides, when $\eta = -1000$, the reverse flow forms near an inner cylinder wall and it diminishes by increasing the value of ξ parameter.

6.2.2. Wall velocity changes

Considering the no-slip condition, changes in the velocity of cylinder walls influence fluid flow. As can be seen in Figure 5, the effect of changes in the velocity of inner cylinder walls is presented in two states of $= \mp 1000$. In Figure 6(a) and in the case of $\eta = +1000$, increasing the velocity of the inner wall intensifies reverse flow. However, increasing the velocity of this wall reduces and eventually reverse flow disappears in

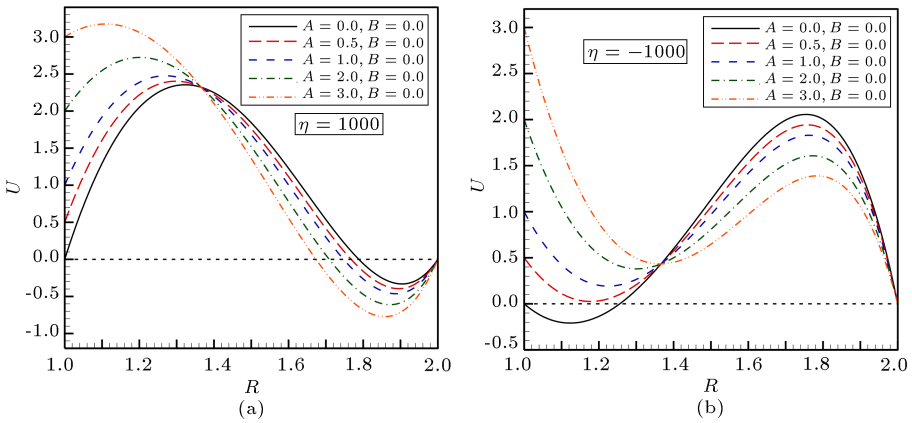

Figure 5. Dimensionless velocity changes in different states of the movement of inner cylinders' walls in $\eta = \pm 1000$, $\xi = 0.2$, $Ha = 5.0$, $S = -1.0$, and $\lambda = 2.0$.

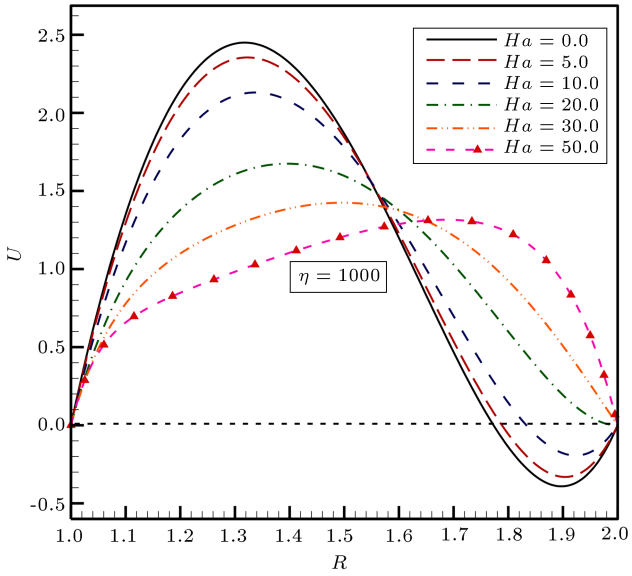

Figure 6. Dimensionless velocity changes at different values of Ha in $\eta = 1000$, $A = 0$, $B = 0$, $\xi = 0.2$, $S = -1.0$, and $\lambda = 2.0$.

the state of $\eta = -1000$ (Figure 6(b)). According to Figure 5, it is worth mentioning that increasing the wall velocity more than its critical value is regarded as the productive factor of reverse flow.

6.2.3. Magnetic field

Figure 6 depicts the effect of magnetic field changes on dimensionless velocity in the radial space between two cylinders. With regard to momentum equations (Relation (7)), it can be seen that buoyancy and Lorentz forces are in opposite directions. As indicated in Figure 6, increasing the magnetic field causes Lorentz force to overcome buoyancy force and thus, eliminates the reverse flow. In fact, applying the magnetic field stabilizes the flow. At large Hartman numbers, the dimensionless velocity profile takes the flat form and reverse flow will completely disappear. Therefore, the application of the magnetic field can be considered as one of the effective methods for eliminating reverse flow.

6.2.4. Suction/injection

Dimensionless velocity in the radial distance between two cylinders in various suction/injection parameters is shown in Figure 7. Figure 7(a) surveys the situation in which $S > 0$. In this case, with the enhancement of S, the fluid volume near the wall of outer cylinder increases and the maximum velocity is drawn toward the inner cylinder wall. As can be seen in this figure, increasing S causes reverse flow to disappear. In Figure 7(b), the dimensionless velocity profile is drawn in the radial distance between the two inner and outer cylinders in $S < 0$. It is evident that as the value of S decreases, the volume of fluid increases near the outer wall and the maximum velocity is drawn toward the outer cylinder wall and the reverse flow disappears. Therefore, suction/injection can be considered as a factor to eliminate reverse flow. In other words, the optimum way to eliminate reverse flow through suction/injection is to increase the volume of fluid near the wall where reverse flow occurs.

6.2.5. Volume fraction of hybrid nanofluid

According to Tables 1 and 2, by increasing the volume fraction of nanoparticles in the base fluid, thermophysical properties of hybrid nanofluid including thermal conductivity, density, dynamic viscosity, and heat capacity are enhanced. Increasing these parameters affects the velocity of hybrid nanofluid. Dimensionless velocity change in the distance between inner and outer cylinders for base fluid ($\varphi = 0$) and hybrid nanofluid with volume fractions of 0.1% and 0.3% in two states of $\eta = \mp 1000$ is demonstrated in Figure 8. As can be seen, increasing the volume fraction of nanoparticles in base fluid increases fluid velocity near the cold wall and decreases it near the hot wall in two states of $\eta = \mp 1000$. Accordingly, increasing φ can help reverse flow to reduce.

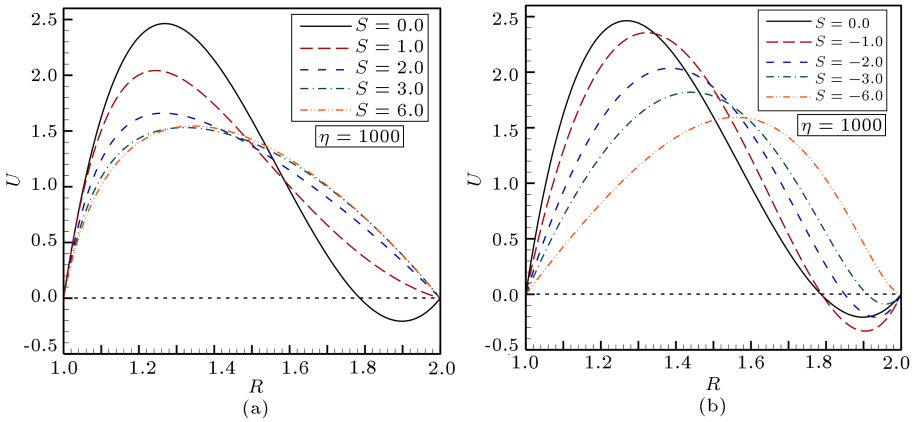

Figure 7. Dimensionless velocity changes at different values of S in $\eta = 1000$, $A = 0$, $B = 0$, $\xi = 0.2$, $Ha = 5.0$, and $\lambda = 2.0$.

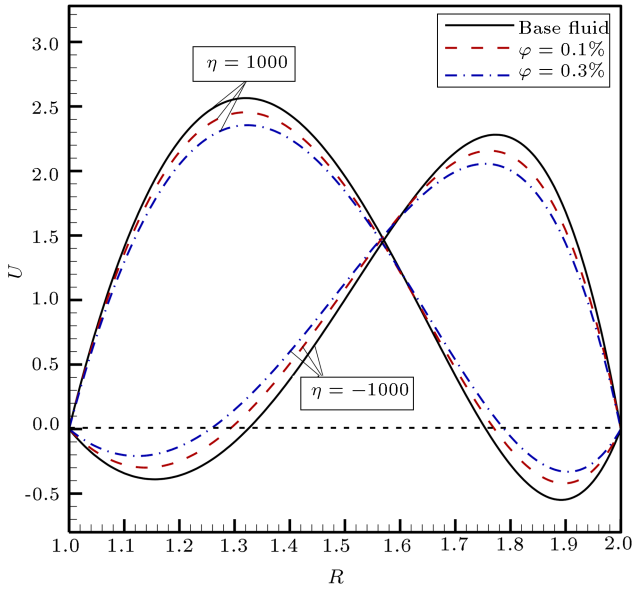

Figure 8. Dimensionless velocity changes at different values of φ in $\eta = \pm 1000$, $A = 0$, $B = 0$, $\xi = 0.2$, $Ha = 5.0$, $S = -1.0$, and $\lambda = 2.0$.

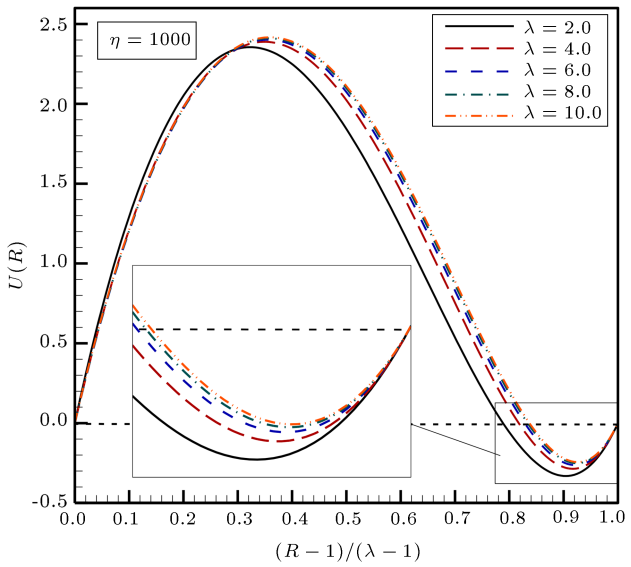

Figure 9. Dimensionless velocity changes vs. $(R-1)/(\lambda-1)$ at different values of λ in $\eta = 1000$, $A = 0$, $B = 0$, $\xi = 0.2$, $Ha = 5.0$, and $S = -1.0$.

6.2.6. Ratio of radius

Dimensionless velocity changes in the space between two cylinders at different ratios of radius are plotted in Figure 9. For a better comparison, the horizontal axis was normalized in the form of $(R-1)/(\lambda-1)$. In fact, rising the radius ratio increases the distance between the two cylinders and this action influences fluid flow velocity between the two cylinders. As can be observed in Figure 9, increasing the ratio of radius parameter can change the velocity of fluid and reduce reverse flow.

7. Analysis of heat transfer and shear stress

The dependence of Nusselt number and dimensionless shear stress on φ for the cylinder walls for two states of $\eta = \pm 100$ is presented in Table 5. As can be seen, adding the nanoparticles of MWCNT-Fe_3O_4 in the base fluid increases Nusselt number and shear stress on both walls. The coefficient of thermal conductivity in hybrid nanofluid is increased by enhancing volume fraction and, thus, heat distribution in the hybrid nanofluid will take place better by increasing heat diffusivity from annulus walls to the space between them. Therefore, in this study, $\varphi = 0.3\%$ was used as a state in which a heat transfer rate was maximum.

8. Critical values in determining reverse flow

Tables 6 and 7 shows a better and more accurate study of the effect of changes in different parameters on reverse flow. In these tables, critical values are given for mixed convection parameter (η_{cr}) with the change of various parameters for two states of $\eta < 0$ and $\eta > 0$. $\xi = 0$ indicates the maximum temperature difference between the inner and outer walls of cylinders, and as ξ gets closer to 1, the temperature of two walls approaches symmetrical temperature conditions. The quantity R_{cr} represents the radius at which reverse flow occurs. In addition, the values of Nusselt number and dimensionless shear stress corresponding to η_{cr} were calculated on the walls of the cylinders. The data obtained in this table confirm previous results. According to Tables 6 and 7, if $|\eta_{cr}|$ has larger values, flow condition is given such that the reverse flow is unlikely to happen. Regarding Table 6, increasing the parameters of ξ, $|S|$, Ha, λ, and φ leads to the increase in the value of $|\eta_{cr}|$. Therefore, the occurrence of reverse flow can be prevented by increasing these

Table 5. The values of Nusselt number and dimensionless shear stress for different volume fractions in $A = 0$, $B = 0$, $\xi = 0.2$, $Ha = 5.0$, $S = -1.0$, $\lambda = 2.0$.

Variable parameter	$\eta = +100$				$\eta = -100$			
	Nu_1	τ_1	Nu_λ	τ_λ	Nu_1	τ_1	Nu_λ	τ_λ
$\varphi = 0.0$	0.963	7.172	7.583	−4.673	0.824	4.921	8.061	−8.190
$\varphi = 0.1$	1.317	8.298	7.965	−5.513	1.154	5.856	8.440	−9.016
$\varphi = 0.3$	1.361	9.178	8.072	−6.214	1.207	6.692	8.509	−9.711

Table 6. The critical values of η in $A = 0, B = 0, \xi = 0.2, Ha = 5.0, S = -1.0, \lambda = 2.0$.

Variable parameter	$R_{cr} = 1, \eta < 0, \tau_1 = 0$				$R_{cr} = \lambda, \eta > 0, \tau_\lambda = 0$			
	η_{cr}	Nu_1	Nu_λ	τ_λ	η_{cr}	Nu_1	τ_1	Nu_λ
$\xi = 0.0$	−510.610	0.926	9.959	−19.124	364.293	1.758	13.596	7.397
$\xi = 0.2$	**−638.263**	**0.926**	**9.959**	**−19.124**	**455.366**	**1.758**	**13.596**	**7.397**
$\xi = 0.3$	−729.443	0.926	9.959	−19.124	520.419	1.758	13.596	7.397
$\xi = 0.4$	−851.017	0.926	9.959	−19.124	607.155	1.758	13.596	7.397
$\xi = 0.6$	−1276.525	0.926	9.959	−19.124	910.733	1.758	13.596	7.397
$\xi = 0.8$	−2553.050	0.926	9.959	−19.124	1821.466	1.758	13.596	7.397
$Ha = 0.0$	−604.436	0.936	9.885	−18.432	416.600	1.767	13.352	7.385
$Ha = 5.0$	**−638.263**	**0.926**	**9.959**	**−19.124**	**455.366**	**1.758**	**13.596**	**7.397**
$Ha = 10.0$	−742.729	0.901	10.166	−21.110	568.970	1.732	14.304	7.429
$Ha = 20.0$	−1179.636	0.836	10.809	−27.948	994.559	1.661	16.813	7.523
$Ha = 30.0$	−1906.706	0.783	11.491	−36.752	1646.074	1.595	20.195	7.620
$Ha = 50.0$	−4098.365	0.723	12.539	−55.886	3545.359	1.507	27.936	7.767
$S = 6.0$	−2485.034	66.979	0.000	−5.700	34768.802	71.661	243.625	0.000
$S = 3.0$	−1042.806	33.904	0.039	−7.135	6703.659	37.290	90.020	0.006
$S = 2.0$	−725.803	23.109	0.343	−8.112	3037.212	26.098	56.622	0.087
$S = 1.0$	−512.311	12.924	1.775	−9.889	1222.166	15.513	33.259	0.756
$S = 0.0$	−457.981	4.827	5.148	− 13.324	579.033	6.771	19.990	3.192
$S = -1.0$	**−638.263**	**0.926**	**9.959**	**−19.124**	**455.366**	**1.758**	**13.596**	**7.397**
$S = -2.0$	−1090.158	0.093	15.374	−27.031	503.201	0.250	10.440	12.397
$S = -3.0$	−1818.686	0.006	20.987	−36.409	611.357	0.023	8.614	17.682
$S = -6.0$	−5929.580	0.000	38.157	−71.709	1108.554	0.000	5.781	34.027
$\varphi = 0.0$	−537.354	0.626	9.351	−15.879	365.788	1.242	10.163	7.029
$\varphi = 0.1$	−579.429	0.889	9.848	−17.411	414.842	1.694	12.144	7.317
$\varphi = 0.3$	**−638.263**	**0.926**	**9.959**	**−19.124**	**455.366**	**1.758**	**13.596**	**7.397**
$\lambda = 2.0$	**−638.263**	**0.926**	**9.959**	**−19.124**	**455.366**	**1.758**	**13.596**	**7.397**
$\lambda = 4.0$	−771.060	0.114	12.640	−6.965	444.039	0.260	4.262	9.796
$\lambda = 6.0$	−829.583	0.028	13.604	−4.296	445.218	0.068	2.580	10.654
$\lambda = 8.0$	−861.417	0.010	14.099	−3.109	446.600	0.025	1.878	11.092
$\lambda = 10.0$	−881.409	0.004	14.401	−2.437	447.635	0.011	1.489	11.357

parameters. As can be seen, the changes in ξ parameter do not have a significant effect on shear stress and Nusselt number, but $|\eta_{cr}|$ increases with its enhancement. The negative values of shear stress also indicate that the slope of velocity is negative in regions near the wall of cylinder. As already mentioned, if the values of $|\eta_{cr}|$ in Tables 6 and 7 are larger, the effective parameter in $|\eta_{cr}|$ has a noticeable role in eliminating reverse flow. For example, such parameters as Hartman number, suction/injection parameter, and dimensionless temperature difference are among the parameters that have a more significant effect on disappearing reverse flow. According to Table 7 and considering the larger values for $|\eta_{cr}|$, it can be stated that the movement of the inner cylinder wall in case of $\eta < 0$ and the movement of the outer wall in case of $\eta > 0$ are regarded as the most effective methods for overcoming reverse flow.

9. Conclusions

In this research, exact solution results were presented for hydrothermal behavior of Multi Walled Carbon Nanotube (MWCNT)-Fe_3O_4 hybrid nanofluid in a vertical cylindrical annulus by considering radial magnetic field, suction/injection, and moving walls. Results demonstrated that adding hybrid nanoparticles to base

Table 7. The effect of increasing the velocity of inner and outer cylinder walls on η_{cr} in $\xi = 0.2$, $Ha = 5.0$, $S = -1.0$, $\lambda = 2.0$.

Variable	$\eta < 0$						$\eta > 0$					
A and B	R_{cr}	η_{cr}	Nu_1	Nu_γ	τ_1	τ_λ	R_{cr}	η_{cr}	Nu_1	τ_1	Nu_γ	τ_λ
$A = 0.0, B = 0.0$	**1.000**	**−638.263**	**0.926**	**0.000**	**9.959**	**−19.124**	**2.000**	**455.366**	**1.758**	**13.596**	**7.397**	**0.000**
$A = 0.5, B = 0.0$	1.180	−1024.393	0.835	−7.506	10.826	−24.902	2.000	399.684	1.877	10.198	7.264	0.000
$A = 1.0, B = 0.0$	1.229	−1170.609	0.831	−12.030	10.875	−26.485	2.000	344.001	2.015	6.801	7.136	0.000
$A = 2.0, B = 0.0$	1.288	−1343.315	0.862	−19.588	10.532	−27.558	2.000	232.637	2.359	0.005	6.893	0.000
$A = 3.0, B = 0.0$	1.331	−1431.775	0.929	−26.099	9.939	−27.158	2.000	121.272	2.847	−6.791	6.666	0.000
$A = 0.0, B = 0.0$	**1.000**	**−638.263**	**0.926**	**0.000**	**9.959**	**−19.124**	**2.000**	**455.366**	**1.758**	**13.596**	**7.397**	**0.000**
$A = 0.0, B = 0.5$	1.000	−518.922	0.859	0.000	10.560	−14.153	1.876	940.537	2.075	18.145	7.086	11.368
$A = 0.0, B = 1.0$	1.000	−638.263	0.802	0.000	11.237	−9.182	1.838	1152.392	1.914	19.295	7.228	17.957
$A = 0.0, B = 2.0$	1.000	−399.581	0.707	0.000	12.890	0.760	1.789	1432.294	1.491	19.807	7.797	28.620
$A = 0.0, B = 3.0$	1.000	−160.899	0.632	0.000	15.114	10.703	1.751	1603.096	1.149	18.963	8.720	37.375
$A = 0.0, B = 0.0$	**1.000**	**−638.263**	**0.926**	**0.000**	**9.959**	**−19.124**	**2.000**	**455.366**	**1.758**	**13.596**	**7.397**	**0.000**
$A = 0.5, B = 0.5$	1.188	−880.261	0.787	−7.198	11.435	−19.498	1.871	862.441	2.193	14.468	6.999	10.976
$A = 1.0, B = 1.0$	1.249	−857.762	0.748	−11.108	12.062	−15.246	1.826	973.806	2.078	11.663	7.084	16.782
$A = 2.0, B = 2.0$	1.344	−617.502	0.725	−16.499	12.497	−3.329	1.752	982.254	1.582	3.389	7.639	24.645
$A = 3.0, B = 3.0$	1.477	−52.525	0.787	−17.854	11.433	14.266	1.644	647.717	1.061	−9.148	9.113	26.511

fluid increased Nusselt number and dimensionless shear stress on the inner and outer cylinder walls. Nusselt number on the inner cylinder wall decreases, remains almost constant, and increases with the enhancement of ξ for $\eta > 0$, $\eta = 0$, and $\eta < 0$, respectively. In addition, at a constant ξ, dimensionless shear stress and Nusselt number increased in the case of the inner cylinder wall by increasing η values from negative to positive. On the outer cylinder, these results turned out to be opposite for Nusselt number and were similar in terms of shear stress. Analysis of effective factors and parameters influencing reverse flow led to the following results:

- Increasing the values of wall velocity and $|\eta|$ to more than critical values was taken into account as the factor in creating reverse flow;
- Reverse flow decreased with the enhancement of ξ parameter and it disappeared in the situation of symmetric channel wall heating;
- When $\eta = +1000$, increasing the wall velocity of inner and outer cylinders increased and decreased reverse flow, respectively. The opposite of these results held in the case of $\eta = -1000$. Moreover, the simultaneous movement of both walls could intensify reverse flow;
- Application of magnetic field led to the stability of the flow and reverse flow was completely eliminated at large Hartman numbers;
- In the two states of $\eta = +1000$, $S > 0$ and $\eta = -1000$, $S < 0$, reverse flow disappeared sooner by increasing $|S|$. In other words, the best way to eliminate reverse flow through suction/injection was to increase the volume of fluid near the wall where the reverse flow occurred;
- Increasing the ratio of radius parameter and the volume fraction of nanoparticles in both cases of $\eta = \mp 1000$ led to the reduction of reverse flow;
- Increasing the parameters of ξ, $|S|$, Ha, λ, and φ led to the increase of $|\eta_{cr}|$. If $|\eta_{cr}|$ had larger values, flow condition was such that a reverse flow was unlikely to occur;
- Flow conditions would be better for the lack of reverse flow formation at the center or sides of annulus if $|\eta_{cr}|$ had larger values;
- Parameters such as Hartman number, suction/ injec -tion parameter, and dimensionless temperature difference were among the parameters whose effects on eliminating reverse flow were more significant;
- The movement of the inner cylinder wall when $\eta < 0$ and the movement of the outer wall when $\eta > 0$ were regarded as the most effective methods for overcoming reverse flow.

Nomenclature

A	Coefficient of velocity for inner cylinder
a	Radius of the inner cylinder (m)

B	Coefficient of velocity for outer cylinder
b	Radius of the outer cylinder (m)
B_0	Constant magnetic field (T), $B_m = (B_0 a)/r$
c_p	Specific heat (J/kg K)
D_h	Hydraulic diameter, $D_h = 2(b-a)$
g	Gravitational acceleration (m/s^2)
Ha	Hartman number
k	Thermal conductivity (W/mK)
Nu	Nusselt number
p	Pressure (Pa)
P	Dimensionless pressure
Pr	Prandtl number
Q	Dimensionless volumetric flow rate
R	Axis in the cylindrical coordinates
Re	Reynolds number
S	Suction/injection parameter
T	Hybrid nanofluid temperature (K), $\Delta T = T_1 - T_0$
T_0	Reference temperature (K)
T_1	Wall temperature of inner cylinder (K)
T_2	Wall temperature of outer cylinder (K)
U	Velocity in z direction (m/s)
u_0	Reference velocity (m/s)
u_m	Mean velocity (m/s)
V	Velocity in r direction (m/s)
z	Axis in the cylindrical coordinates

Greek letters

α_T	Thermal diffusivity (m^2/s), $\alpha_T = k/(\rho c_p)$
β	Thermal expansion coefficient (1/K)
ξ	Temperature difference ratio
η	Mixed convection parameter
θ	Dimensionless temperature of nanofluid
λ	Ratio of the radius between two cylinders
μ	Dynamic viscosity (kg/ms)
ρ	Density (kg/m^3)
v	Kinematic viscosity (m^2/s), $\nu = \mu/\rho$
σ	Electrical conductivity ($m^{-1}\Omega^{-1}$)
τ	Dimensionless shear stress
φ	Volume fraction

Subscripts

1	Value on inner wall
b	Bulk temperature
hnf	Hybrid nanofluid
f	Pertaining to base fluid
m	Mean value
np	Nano particles
λ	Value on outer wall

References

1. Shakiba, A. and Vahedi, K. "Numerical analysis of magnetic field effects on hydro-thermal behavior of a magnetic nanofluid in a double pipe heat exchanger", *Journal of Magnetism and Magnetic Materials*, **402**, pp. 131–142 (2016).
2. Shakiba, A. and Rahimi, A.B. "Role of movement of the walls with time-dependent velocity on flow and mixed convection in vertical cylindrical annulus with suction/injection", *Scientia Iranica*, **28**(3), pp. 1306–1317 (2020).
3. Husain, S., Adil, M., Arqam, M., et al. "A review on the thermal performance of natural convection in vertical annulus and its applications", *Renewable and Sustainable Energy Reviews*, **150**, 111463 (2021).
4. Oni, M.O., Jha, B.K., and Ajibade, A.O. "Interplay of dual streaming potentials on electroosmotic mixed convection flow in a vertical microannulus with Joule heating effect", *International Communications in Heat and Mass Transfer*, **131**, 105839 (2022).
5. Jha, B.K. and Gambo, D. "Theoretical investigation on the impact of an oscillating time-dependent pressure gradient on Dean flow in a porous annulus", *Propulsion and Power Research*, **10**(3), pp. 294–302 (2021).
6. Alsharif, A.M. and Abd Elmaboud, Y. "Electroosmotic flow of generalized fractional second grade fluid with fractional Cattaneo model through a vertical annulus", *Chinese Journal of Physics*, **77**, pp. 1015–1028 (2021).
7. Jha, B.K. and Gambo, D. "Hydrodynamic behaviour of velocity of applied magnetic field on unsteady MHD Couette flow of dusty fluid in an annulus", *The European Physical Journal Plus*, **137**(1), p. 67 (2022).
8. Girish, N., Sankar, M., and Keerthi, R. "Analysis of fully developed mixed convection in open-ended annuli with viscous dissipation", *Journal of Thermal Analysis and Calorimetry*, **143**(1), pp. 503–521 (2021).
9. Jha, B.K. and Yusuf, T.S. "Transient Taylor-Dean flow in a composite annulus with porous walls partially filled with porous material", *Journal of the Egyptian Mathematical Society*, **30**(1), p. 2 (2022).
10. Amouzadeh, F., Tondro, M., Asadi, Z., et al. "Suction and injection effect on magnetohydrodynamic fluid flow within a vertical annulus for electrical wire cooling", *Case Studies in Thermal Engineering*, **27**, 101241 (2021).
11. Wang, F., Xu, Y.P., Qahiti, R., et al. "Simulation of hybrid nanofluid flow within a microchannel heat sink

considering porous media analyzing CPU stability", *Journal of Petroleum Science and Engineering*, **208**, 109734 (2022).

12. Shoeibi, S., Kargarsharifabad, H., Rahbar, N., et al. "Performance evaluation of a solar still using hybrid nanofluid glass cooling-CFD simulation and environmental analysis", *Sustainable Energy Technologies and Assessments*, **49**, 101728 (2022).
13. Asadi, A., Zaboli, M., Mogharrebi, A.R., et al. "Numerical analysis of turbulence-inducing elements with various geometries and utilization of hybrid nanoparticles in a double pipe heat exchanger", *Alexandria Engineering Journal*, **61**(5), pp. 3633–3644 (2022).
14. Thriveni, K. and Mahanthesh, B. "Sensitivity analysis of nonlinear radiated heat transport of hybrid nanoliquid in an annulus subjected to the nonlinear Boussinesq approximation", *Journal of Thermal Analysis and Calorimetry*, **143**(3), pp. 2729–2748 (2021).
15. Malvandi, A., Moshizi, S., Soltani, E.G., et al. "Modified Buongiorno's model for fully developed mixed convection flow of nanofluids in a vertical annular pipe", *Computers and Fluids*, **89**, pp. 124–132 (2014).
16. Shakiba, A. and Baradaran Rahimi, A. "Mixed convective flow of electrically conducting fluid in a vertical cylindrical annulus with moving walls adjacent to a radial magnetic field along with transpiration", *Journal of Fluids Engineering*, **141**(8), 081111 (2019).
17. Shakiba, A. and Baradaran Rahimi, A. "Nanofluid flow and MHD mixed convection inside a vertical annulus with moving walls and transpiration considering the effect of Brownian motion and shape factor", *Journal of Thermal Analysis and Calorimetry*, **138**(1), pp. 501–515 (2019).
18. Jha, B. and Aina, B. "Impact of induced magnetic field on magnetohydrodynamic (MHD) natural convection flow in a vertical annular micro-channel in the presence of radial magnetic field", *Propulsion and Power Research*, **7**(2), pp. 171–181 (2018).
19. Kazakidi, A., Plata, A., Sherwin, S., et al. "Effect of reverse flow on the pattern of wall shear stress near arterial branches", *Journal of the Royal Society Interface*, **8**(64), pp. 1594–1603 (2011).
20. Magyari, E. and Chamkha, A.J. "Combined effect of heat generation or absorption and first-order chemical reaction on micropolar fluid flows over a uniformly stretched permeable surface: The full analytical solution", *International Journal of Thermal Sciences*, **49**(9), pp. 1821–1828 (2010).
21. Barletta, A. "Combined forced and free flow of a power-law fluid in a vertical annular duct", *International Journal of Heat and Mass Transfer*, **43**(19), pp. 3673–3686 (2000).
22. Jha, B.K. and Oni, M.O. "Theory of fully developed mixed convection including flow reversal: A nonlinear Boussinesq approximation approach", *Heat Transfer-Asian Research*, **48**(8), pp. 3477–3488 (2019).
23. Jha, B.K. and Aina, B. "Role of suction/injection on steady fully developed mixed convection flow in a vertical parallel plate microchannel", *Ain Shams Engineering Journal*, **9**(4), pp. 747–755 (2018).
24. Jha, B.K. and Oni, M.O. "Mixed convection flow in a vertical channel with temperature dependent viscosity and flow reversal: An exact solution", *International Journal of Heat and Technology*, **36**(2), pp. 607–613 (2018).
25. Jha, B.K. and Aina, B. "Mathematical modelling and exact solution of steady fully developed mixed convection flow in a vertical micro-porous-annulus", *Afrika Matematika*, **26**(7), pp. 1199–1213 (2015).
26. Jha, B.K., Oni, M.O., and Aina, B. "Steady fully developed mixed convection flow in a vertical micro-concentric-annulus with heat generating/absorbing fluid: An exact solution", *Ain Shams Engineering Journal*, **9**(4), pp. 1289–1301 (2018).
27. Mahian, O., Kolsi, L., Amani, M., et al. "Recent advances in modeling and simulation of nanofluid flows-Part I: Fundamentals and theory", *Physics Reports*, **790**, pp. 1–48 (2019).
28. Sundar, L.S., Singh, M.K., and Sousa, A.C. "Enhanced heat transfer and friction factor of MWCNT-Fe_3O_4/water hybrid nanofluids", *International Communications in Heat and Mass Transfer*, **52**, pp. 73–83 (2014).
29. Mehryan, S.A.M., Sheremet, M.A., Soltani, M., et al. "Natural convection of magnetic hybrid nanofluid inside a double-porous medium using two-equation energy model", *Journal of Molecular Liquids*, **277**, pp. 959–970 (2019).

Biographies

Ali Shakiba received his PhD in Mechanical Engineering from Faculty of Mechanical Engineering at Ferdowsi University of Mashhad, Iran in 2020. He is currently a research fellow at Optoelectronics Research Centre at University of Southampton, United Kingdom. His research interests include fluid flow and heat transfer analysis and optimization, mathematical and numerical modeling, hollow core optical fiber, and biomechanics.

Asghar Baradaran Rahimi was born in Mashhad, Iran, in 1951. He received his BSc degree in Mechanical Engineering from Tehran Polytechnic in 1974 and a PhD degree in Mechanical Engineering from the University of Akron, Ohio, USA in 1986. He has been a Professor at the Department of Mechanical Engineering at Ferdowsi University of Mashhad since 2001. His research and teaching interests include heat transfer and fluid dynamics, gas dynamics, continuum mechanics, applied mathematics, and singular perturbation.